

Electrical Conductivity of Zeolite Films: Influence of Charge Balancing Cations and Crystal Structure

Mercedes Álvaro, Jose F. Cabeza, David Fabuel, Hermenegildo García,*
Enrique Guijarro,* and José Luís Martínez de Juan

*Instituto de Tecnología Química CSIC-UPV and Departamento de Ingeniería Electrónica,
Universidad Politécnica de Valencia, Avda. de Los Naranjos s/n, 46022 Valencia, Spain*

Received March 2, 2005. Revised Manuscript Received October 27, 2005

The electrical conductivity of a series of zeolites varying the charge balancing cation, the crystal structure, and the water content has been measured. The current intensity versus voltage profiles of cells constructed with a conductive glass indium tin oxide anode, an aluminum cathode, and a 50 μm zeolite layer were highly reproducible. Typically, zeolites exhibit a semiconductor profile, dramatically increasing the electrical conductivity from the initial insulator regime to a conductive regime at breaking voltages between 3.5 and 5 V. By adsorbing on the external surface ruthenium trisbipyridyl, we have assessed that the global electrical conductivity of the zeolite films depends on both the external and internal parameters of the zeolite. The fact that the overall electrical conductivity has a component due to the intraparticle conductivity is relevant in the context of developing applications for zeolite-encapsulated guests in nanotechnology.

Introduction

Zeolites have found real application as solid catalysts in industrial processes on a multiton scale in the preparation of both bulk and fine chemicals.^{1,2} Also, zeolites are commercially used as ion exchangers, water softeners, and adsorbents.^{3,4} In contrast to today's economical importance of zeolites in many chemical sectors, most of the promises of zeolites in nanotechnology have not yet been realized.^{5–9} Thus, although zeolites have been one of the preferred host materials for occluding organic guests,^{10–16} the potential of supramolecular host–guest assemblies based on zeolites and related porous inorganic hosts has not yet been applied for

the preparation of advanced materials for some commercial applications. This is in spite of there being many examples in the literature, showing that the “molecular” properties of a guest are very frequently altered as result of its confinement in a restricted space and by the presence of zeolite-active sites near the encapsulated guest.^{17–20}

The application of supramolecular zeolite systems in the field of photonics could be, in principle, simpler to achieve as a result of the transparency of the zeolite framework in most of the UV–vis wavelengths, thus allowing the excitation of the incorporated guests inside the zeolite. This transparency of the zeolite framework also permits monitoring of the corresponding guest response. Thus, the observation of lasing generated through a whispering gallery mode upon light excitation of the dye molecules adsorbed inside microcrystals of zeolites and related aluminophosphates has been reported.^{9,21,22}

In contrast to photonic devices, where no mechanical contact between the supramolecular zeolitic material and other components of the device is needed, applications of zeolite-based supramolecular systems in electronics are considerably more complicated because an electrical contact between external electrodes and the internally encapsulated guests is necessary in order to observe the expected response.

In addition, there is still much work to do to harness the electrical conductivity behavior of zeolites that are generally

* Corresponding authors. E-mail: hgarcia@quim.upv.es (H.G.), eguijarro@eln.upv.es (E.G.).

- (1) *Introduction to Zeolite Science and Practice*; van Bekkum, H., Flanigen, E. M., Jansen, J. C., Eds.; Elsevier: Amsterdam, 1991.
- (2) Corma, A.; Garcia, H. *Chem. Rev.* **2003**, *103*, 4307–4365.
- (3) Barrer, R. M. *Zeolites and Clay Minerals as Sorbents and Molecular Sieves*; Academic Press: London, 1978.
- (4) Breck, D. W. *Zeolite Molecular Sieves: Structure, Chemistry and Use*; John Wiley and Sons: New York, 1974.
- (5) Bruhwiler, D.; Calzaferri, G. *Microporous Mesoporous Mater.* **2004**, *72*, 1–23.
- (6) Calzaferri, G. *Chimia* **1998**, *52*, 525–532.
- (7) Corma, A.; Garcia, H. *Chem. Commun.* **2004**, 1443–1459.
- (8) Herron, N. J. *Inclusion Phenom. Mol. Recognit. Chem.* **1995**, *21*, 283–98.
- (9) Hoffmann, K.; Marlow, F. *Handb. Zeolite Sci. Technol.* **2003**, 921–949.
- (10) Calzaferri, G.; Glaus, S.; Leiggenger, C.; Kuge, K. I. *Host–Guest Syst. Nanoporous Cryst.* **2003**, 424–450.
- (11) Calzaferri, G.; Huber, S.; Maas, H.; Minkowski, C. *Angew. Chem., Int. Ed.* **2003**, *42*, 3732–3758.
- (12) Corma, A.; Garcia, H. *Dalton* **2000**, 1381–1394.
- (13) Corma, A.; Garcia, H. *Eur. J. Inorg. Chem.* **2004**, 1143–1164.
- (14) De Vos, D. E.; Jacobs, P. A. *Stud. Surf. Sci. Catal.* **2001**, *137*, 957–985.
- (15) Dutta, P. K. J. *Inclusion Phenom. Mol. Recognit. Chem.* **1995**, *21*, 215–37.
- (16) *Photochemistry in Organized and Constrained Media*; Ramamurthy, V., Ed.; VCH: New York, 1991.

- (17) Ramamurthy, V. *Chimia* **1992**, *46*, 359–376.
- (18) Szulbinski, W. S.; Manuel, D. J.; Kincaid, J. R. *Inorg. Chem.* **2001**, *40*, 3443–3447.
- (19) Schulz-Ekloff, G.; Wohrle, D.; van Duffel, B.; Schoonheydt, R. A. *Microporous Mesoporous Mater.* **2002**, *51*, 91–138.
- (20) Scaiano, J. C.; Garcia, H. *Acc. Chem. Res.* **1999**, *32*, 783–793.
- (21) Marlow, F. *Mol. Cryst. Liq. Cryst. Sci. Technol., Sect. A* **2000**, *341*, 289–294.
- (22) Marlow, F.; Dong, W. T.; Hoffmann, K.; Loerke, J. *Handb. Porous Solids* **2002**, *5*, 3029–3063.

classified as insulators. The electrical conductivity in hydrated faujasites and zeolite dispersions has been ascribed to the movement of ions inside supercage and sodalite cages.^{23–26} According to these reports, the charge-compensating cations moved through the zeolite voids by overcoming potential barriers of different heights. Ionic diffusion should depend on the structure and composition of the zeolite and the charge nature of the charge-balancing cation. However, for many applications in nanotechnology, it would be of interest to obtain thin zeolite films exhibiting sufficient conductivity at relatively low dc voltages. Clearly, more information is needed about electrical conductivity in thin films depending on the zeolite sample.

As an example of the interest in determining the conductivity of zeolite films, we have become involved in a project aimed at the development of light emitting diodes (LEDs) based on zeolite-encapsulated electroluminescent guests.^{27,28} In this application, to observe electroluminescence from the adsorbed organic guest, the migration of electrons and holes from the external working electrodes toward the interior of the zeolite particles, where electrons and holes should collapse on the encapsulated guest producing the electroluminescent excited state, is necessary. It is not obvious if electrical conductivity in zeolites could be related to the movement of electrons or if it is due to ion movement. In the latter case, the relevance to LED operation would be minimal.

For the development of microelectronic applications of zeolite host–guest systems, the prior determination of the electrical conductivity of zeolite films is necessary in order to understand the factors influencing this conductivity. The long-term goal is to find the optimum zeolite materials that minimize or even reverse the negative impact of the inert zeolite matrix on the electrical conductivity.

In this work, we have prepared films of a series of zeolites differing on the nature of the charge-balancing cation as well as in the zeolite structure and proceeded to measure their electrical conductivity for direct currents. The results have shown that micrometric zeolite films between two conducting electrodes in the absence of a liquid electrolyte behave, under certain conditions, as semiconductors, the breaking voltage in conductivity being significantly dependent on the nature of the charge-balancing cation and on the zeolite structure. However, the electrical conductivity measured for our samples may be unrelated to the intrazeolite conduction of electrons and holes and may be exclusively related to an ion transport mechanism. Nevertheless, our data are a necessary step before a complete understanding of the zeolite electric conductivity mechanism can be achieved.

Experimental Section

Materials. NaY(2.7) was a commercial sample (PQ, CBV 100). The other alkali metal ion Y zeolites were obtained starting from NaY(2.7) by ion exchange. Approximately 10 mL of a 1 M aqueous solution of $M(\text{AcO})_n$ ($M = \text{Li, K, Rb, Cs, or Co}$) was prepared. Then, 1 g of NaY(2.7) zeolite was added, and the resulting suspension was stirred at 80 °C for 5 h. After this time, the solid was filtered and washed copiously with distilled water. The resulting partially exchanged white solid was submitted to a subsequent treatment with another 10 mL of a 1 M aqueous $M(\text{AcO})_n$ solution. The heating and filtration steps were performed as before. This whole ion exchanging process was repeated a third time to ensure the maximum Na^+ exchange. Finally, the white powder was calcined at 400 °C for 5 h in the open atmosphere. The temperature program for calcinations was 5 °C/min, 400 °C for 5 h.

Dealuminated USY zeolites were obtained starting from NaY by steaming at 350 °C for 2 h. Then, the zeolite was exhaustively washed with a 0.1 M solution of $(\text{NH}_4)_2\text{SiF}_6$ and ion exchanged with NH_4AcO or NaAcO as described above.

SiO_2 was a commercial sample (Aerosil 300). CeO_2 was obtained by dissolving 0.5 g of $\text{Ce}(\text{NO}_3)_4$ in 25 mL of distilled water previously acidified by the addition of 0.3 mL of concentrated HNO_3 . After complete dissolution of the $\text{Ce}(\text{NO}_3)_4$ salt, NH_4OH was added dropwise. $\text{SiO}_2 \cdot \text{CeO}_2$ was prepared starting from a clear aqueous solution of tetraethyl orthosilicate (0.25 g) and $\text{Ce}(\text{NO}_3)_4$ (0.25 g) and performing the cocondensation under basic conditions using a concentrated aqueous solution of ammonium hydroxide. CeO_2 and $\text{SiO}_2 \cdot \text{CeO}_2$ were exhaustively washed with distilled water and dried in an oven at 60 °C before using.

Cell Preparation for Electrical Conductivity Measurements.

Aluminum and conductive transparent indium tin oxide (ITO) glass were used as working electrodes. The ITO glass was cleaned by ultrasonic irradiation in an acetone bath over 5 h. The aluminum surface was exhaustively polished with sandpaper before the preparation of the cell. A $1 \times 1 \text{ cm}^2$ area was defined on the ITO glass using adhesive tape. A suspension of zeolite in ethanol was deposited using a razor blade on the ITO surface. After spreading the zeolite suspension and letting the ethanol evaporate, the zeolite-contaminated adhesive tape was replaced by clean tape. In this way, a homogeneous $1 \times 1 \text{ cm}^2$ zeolite film of about 50 μm thickness was obtained. The adhesive tape around the solid material avoids short-circuiting between aluminum and ITO electrodes. Finally, the counter aluminum electrode was put on top of the dry zeolite film. Optical microscopy reveals that the films are free from pinholes and cracks and that the zeolite particles are uniformly distributed through the electrodes.

Electrical Conductivity Measurement System. Basically, the measurement system contains an acquisition card from National Instruments, model NI6014, and an electronic system formed by the following components: a voltage-to-current converter from Burr-Brown (XTR110) and a voltage attenuator based on the INA146 model from Texas Instruments. The virtual acquisition system was developed on LabView 6.1, also from National Instruments. When this application was used, a voltage ramp was generated with the acquisition card; this voltage was converted to current with the voltage-to-current converter, which was applied to the cell. The voltage developed by the cell is then recorded. To avoid values higher than the card limits (10 V), the voltage was reduced by 10, through the attenuator circuit. A current sweep was made for each intensity–voltage (I – V) pair value, taking care that the values were always within the response range of our system (intensity ranging from 0 to 20 mA and voltage from 0 to 40 V). A four-wire measurement system (see Figure 1) was used to avoid the errors produced by the wire resistances in voltage measurements.

(23) Schoonheydt, R. A.; De Wilde, W.; Velghe, F. *J. Phys. Chem.* **1976**, *80*, 511.

(24) Freeman, D. C., Jr.; Stamires, D. N. *J. Chem. Phys.* **1961**, *35*, 799–806.

(25) Schoonheydt, R. A.; Uytterhoeven, J. B. *Adv. Chem. Ser.* **1971**, *101*, 456–72.

(26) Schoonheydt, R. A.; De Wilde, W.; Velghe, F. *J. Chem. Phys.* **1976**, *80* (5), 511–18.

(27) Alvaro, M.; Corma, A.; Ferrer, B.; Galletero, M. S.; Garcia, H.; Peris, E. *Chem. Mater.* **2004**, *16*, 2142–2147.

(28) Corma, A.; Diaz, U.; Ferrer, B.; Fornes, V.; Galletero, M. S.; Garcia, H. *Chem. Mater.* **2004**, *16*, 1170–1176.

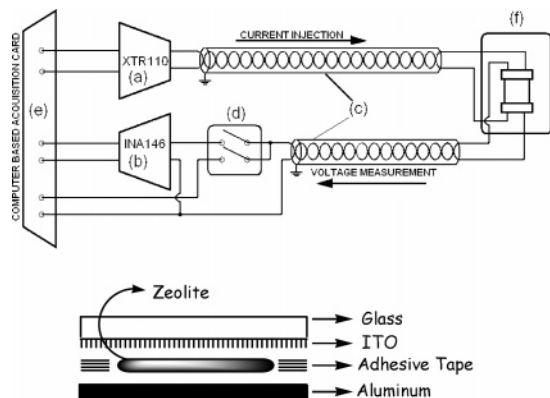


Figure 1. Schematic of the electrical conductivity measurement device and multilayer configuration of the cell used for the measurement of ambient-equilibrated zeolite films. The components of the acquisition system are (a) voltage-to-current converter, (b) voltage reductor, (c) four-wire measurement system, (d) calibration switch, (e) National Instruments acquisition card, and (f) sample cell.

This four-wire setup uses two wires for the current injection and the remaining two for measuring the voltage on the cell. As no current flows through the voltage wires, the error of the voltage measurement is negligible. The choice of current sweep in combination with the four-wire configuration for characterizing the cells instead of an alternative voltage sweep allows making measurements at relatively long distances from the cell with essentially no error. For the calibration of the electronic system, we used a calibrated resistor of 0.1% tolerance. Calibration was made by sweeping the resistance in current from 0 to 20 mA and recording the voltage associated at each point of the current, thus obtaining the real transfer function of the voltage-to-current converter. The errors due to the nonlinearities of the XTR110 voltage-to-intensity converter were corrected automatically by appropriate software programming.

Results and Discussion

The list of the zeolites that have been subjected to electrical conductivity measurements as well as their main structural and analytical data are summarized in Table 1.

In the case of the faujasites Y (Si/Al 2.7), the samples were obtained starting from the corresponding Na^+ form by cation exchange in an aqueous solution using the corresponding alkali metal ion acetate salts. Dealuminated Y zeolites (Si/Al 15 or 20) in their ammonium form were exhaustively ion-exchanged with sodium acetate. Na^+ and H^+ mordenites were commercial samples. Na^+ -exchanged β and ZSM-5 zeolites were obtained from the protonic (H β) or ammonium (NH_4 -ZSM5) forms of these zeolites by ion exchange using an aqueous HNaCO_3 solution that should neutralize the Brønsted acid sites by replacing them with Na^+ ions. For the sake of comparison, we have also included in our study three typical metal oxides such as amorphous silica (SiO_2), nanoparticulated ceria (np- CeO_2), and mixed silicon cerium oxide ($\text{SiO}_2 \cdot \text{CeO}_2$). While SiO_2 was a commercial pyrogenic colloidal silica, nanocrystalline ceria was obtained by the hydrolysis, at basic pH, of aqueous solutions of cerium nitrate. The mixed silicon cerium oxide was obtained by the cocondensation of tetraethyl orthosilicate and $\text{Ce}(\text{NO}_3)_3$ in a basic medium. A more detailed preparation procedure can be found in the Experimental Section.

Table 1. Structural and Analytical Data of the Zeolites Used for the Electrical Conductivity Measurements

Structure	Sample	Si/Al (atom ratio)	Surface area (m^2/g)	Crystal size (μm)
Tridirectional	NaX	1.1	800	13
	LiY	2.7	700	0.2 - 0.4
	NaY(2,7)			
	NaY(15)	15	780	
	NaY(20)	20	750	
	KY	2.7	700	
	RbY			
	CsY			
	CoY			
	HY(3)	3	550	
HY(15)	15	630		
HY(20)	20	600		
Monodirectional	H Mordenite	7.5	400	1 - 3
	Na Mordenite	9.5	360	0.1 - 0.5
Bidirectional	H Beta	12.5	730	3 - 6
	Na Beta	12.5	730	3 - 6
Bidirectional	H ZSM-5	75	420	7 - 12
	Na ZSM-5	15	430	7 - 12

Measurements of the electrical conductivity were carried out in a cell having aluminum as a cathode and a transparent conductive ITO surface on a glass substrate as an anode. Figure 1 shows the schematic of the electronic system used to determine the electrical conductivity of the ambient-equilibrated zeolite powders deposited as self-supported dry thin films of 50 μm thickness. Also, Figure 1 shows a schematic of the cells being used.

We selected aluminum and ITO as working electrodes because these electrodes are the most commonly used in many applications in nanotechnology. It is obvious that the electrical conductivity measurements will depend largely on the cell preparation procedure in such a way that the "intrinsic" electronic transport properties of the material could be disguised and obscured by the actual cell preparation conditions. However, given the scarcity of precedents aimed at characterizing the electrical behavior of zeolite films and recognizing the importance of the measurement conditions, we have chosen parameters that we have considered the closest possible to those that will be used later in microelectronics while still providing information about the impact of the chemical parameters on the zeolite electrical conductivity.³⁰

With the previous considerations in mind, films of ambient-equilibrated zeolites were prepared by depositing a thin layer of the corresponding sample suspended in ethanol on the conductive ITO surface and spreading the suspension using the "razor blade" procedure on a $1 \times 1 \text{ cm}^2$ surface. Adhesive tape conveniently placed on the surface was used to delimit the actual surface on which the zeolite film was deposited. The film thickness in the razor blade procedure

(29) Garcia, H.; Roth, H. D. *Chem. Rev.* **2002**, *102*, 3947–4008.

(30) A full account of the electroluminescence of zeolite-based cells will be published elsewhere.

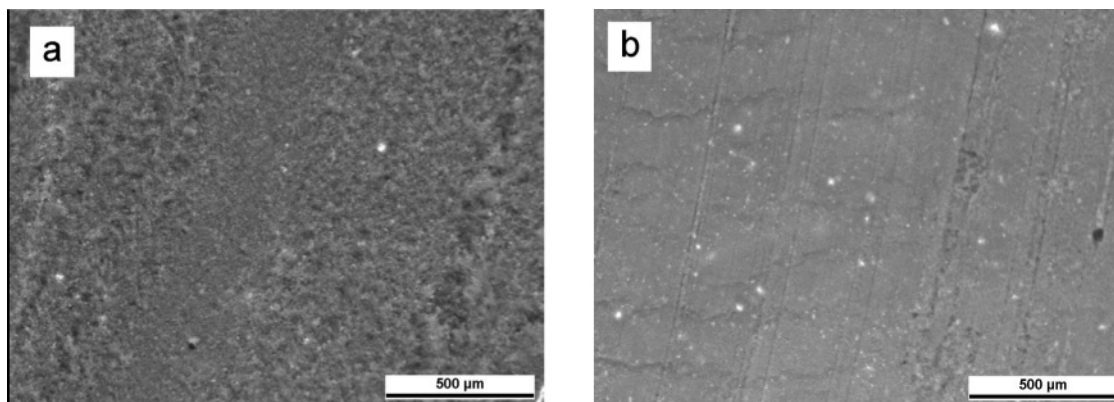


Figure 2. Optical microscopy images of NaY(2.7) (a) and CsY (b) films, prepared by the razor blade procedure.

is related to the thickness of the adhesive tape. In our case, we consistently estimate, by optical microscopy, the layer uniformity and the absence of pinholes and cracks, although some roughness of the surface due to the particulate nature of the material is observable. Selected images illustrating the texture of the films are shown in Figure 2. Also, we use optical microscopy to estimate the thickness to be about 50 μm ; films of this depth are not uncommon for layer thickness in nanotechnology.

After completely drying the solvent in the open air and replacing the adhesive tape with clean tape, the counter aluminum electrode was put on top of the zeolite film and the cell, defined by the zeolite film and the two working electrodes, was held in place by pressing it with two clamps. Each electrode was electrically connected to the measurement device, and the electrical conductivity measurements were controlled by a computer that also provided data storage capability. In addition to the measurement setup for calibration using a precision resistor, blank controls were obtained by preparing cells in the absence of any zeolite in order to determine whether the electrical response of the system was really due to the presence of a zeolite film in the cell. It is worth commenting that, in the absence of any material and using the adhesive tape to avoid short-circuiting, the system does not show any measurable conductivity in the range of direct current voltages studied.

We were initially concerned with the reproducibility and reliability of our electrical measurements. Also, we wanted to demonstrate that the electrical data of our cells really report on the intrinsic chemical properties of the material between the two electrodes. To address reproducibility, we independently prepared several cells of NaY(2.7) zeolite and measured their electrical response many times during the whole period of the electrical conductivity measurements. The data shown in Figure 3 give a visual indication of the reproducibility of our system, clearly supporting that the electrical responses that will be commented upon below are beyond the experimental error of our method. Thus, variations in the electrical response really reflect changes in the intrinsic electrical conductivity of the material of which the film between the electrodes is made. Concerning the relationship between the electrical response and the nature of the material forming the film, Figure 3 shows that, when comparing the general electrical behavior of zeolites with that of ceria, silica, and mixed silicon cerium oxide, it

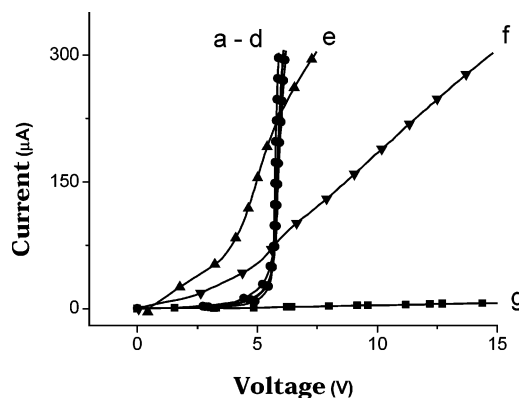


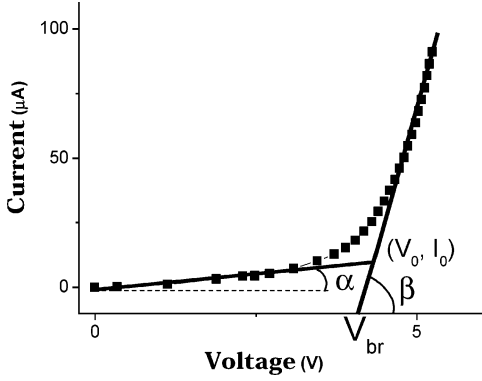
Figure 3. I - V plot comparing zeolite semiconductor behavior with the resistor pattern of other materials: (a-d) NaY(2.7), (e) silicon cerium oxide, (f) cerium oxide, and (g) silica.

becomes apparent that the zeolite films exhibit the typical behavior for a semiconductor, while those of the oxides fit better with a simple resistor.

The electrical conductivity of the zeolite films exhibits ideally two regimes, one at low voltages in which the zeolite film acts basically as an insulator material and one after a breaking voltage where there is a dramatic increase in the conductivity. This semiconductor behavior matches particularly well for the current intensity versus voltage profiles (I - V plots) of alkali metal ion exchanged faujasites (Figure 3), while other zeolites tend to exhibit an intermediate profile between ideal semiconductor and ideal resistor materials. The latter is a material where I is proportional to V , in compliance with the Ohm law.

According to the profile shown in Figure 3 for zeolite NaY(2.7), similar to a semiconductor, the electrical conductivity behavior of different zeolites can be characterized by four parameters, namely, (i) the coordinate of the intercept point of the ideal insulating and conductive straight lines (V_0, I_0), (ii) the breaking voltage (V_{br}), (iii) the slope of the I - V plot in the insulating regime ($1/\tan \alpha$; see Table 2), and (iv) the slope of the I - V plot of the conductive regime ($1/\tan \beta$; see Table 2). The breaking voltage is defined as the voltage of the intersection of the I - V straight line in the conductivity regime. According to these definitions, Table 2 summarizes the data characteristic of the series of zeolites studied, which were obtained from the electrical conductivity measurements.

Table 2. Electrical Conductivity Data Obtained from Several Ion-Exchanged Zeolites^a



sample	(V_0, I_0) (V, A)	V_{br} (V)	$1/\tan \alpha$ (k Ω)	$1/\tan \beta$ (k Ω)
NaX	5.19, 97.62	4.93	603 395	10 452
LiY	4.96, 17.32	4.58	473 933	13 931
NaY(2.7)	5.09, 17.31	4.84	456 621	8 448
NaY(15)	4.63, 12.49	4.42	297 814	7 089
NaY(20)	4.90, 19.78	4.88	222 588	10 378
KY	5.31, 21.56	5.06	537 634	6 547
RbY	5.43, 17.85	5.25	617 283	6 529
CsY	4.14, 16.79	3.89	281 690	13 585
CoY (hydrated)	4.66, 6.74	3.92	1 176 470	155 520
H mordenite ^b				
Na mordenite	3.83, 10.14	3.30	505 050	38 022
H β	7.08, 1.17	3.31	529 100	305 810
Na β	6.31, 2.46	2.00	251 256	151 515
H ZSM-5	7.54, 3.88	4.80	2 083 333	480 769
Na ZSM-5	2.83, 27.21	1.63	92 506	43 103

^a V_{br} , breaking voltage; α and β slopes of the insulating and conductive regimes, respectively; (V_0, I_0), intercept point between the insulator and conductive regimes. ^b This material behaves as an insulator with no measurable conductivity.

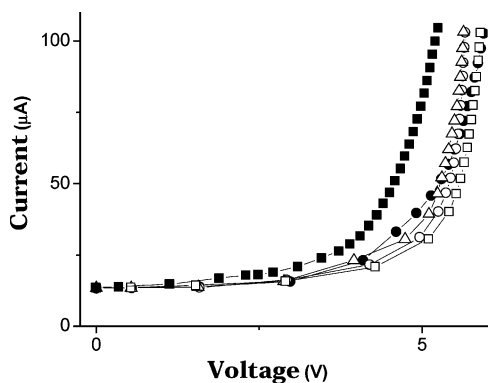


Figure 5. $I-V$ plot of faujasites differing on the framework Si/Al ratio: (a) NaY(2.7), (b) NaY(15), (c) NaY(20), and (d) NaX.

The protonic form (HY) shows a different profile and is, in general, much less conductive than the series of alkali-exchanged Y faujasites. This is not surprising considering that the bond of HX and the Brönsted site is mainly covalent and not purely ionic as in the case of the alkali metal ions. On the other hand, while the $I-V$ plots for Na^+ , K^+ , and Rb^+ -exchanged zeolites are very similar, the behavior of LiY and CsY is significantly different. LiY presents a more resistive pattern with a difference in the slopes of the conductive and insulator regimes of only 34 times. On the other extreme, CsY is the most conductive zeolite and exhibits a breaking point at 3.89 V, which is a voltage significantly smaller than that for the rest of the faujasites. A reasonable assumption to explain the appearance of a breaking voltage and the increase of electric conductivity afterward is that, at these potentials, ions become mobile and leave their defined crystallographic positions. Thus, this breaking voltage will be dependent on the intensity of the interaction between the zeolite aluminosilicate framework and the charge-compensating cation.

Concerning the influence of the framework Si/Al ratio, we studied a series of zeolites having in common the same structure and the nature of the charge-balancing cation, but differing in the framework Si/Al ratio in the range of 1.1–20. The framework aluminum content is an important parameter since it controls the density of the framework negative charges and, therefore, the cation–cation spacing and the energy of the potential barriers for ion jumps. In the case of our zeolite films, the results concerning the influence of the Si/Al ratio were addressed for the faujasite structure, maintaining the same charge-balancing cation. The results are shown in Figure 5, and the values are collected in Table 2.

We have commented above about the reproducibility of our measurements. In this regard, one of the important issues that has always to be considered when working with zeolites is the influence of the water content. In our case, it could be that variations in the zeolite water content could have a significant influence on the electrical conductivity measurements, disguising other analytical and structural parameters. To address the influence of the water content on the electrical measurements, we prepared a cobalt-exchanged Y zeolite.

As it can be seen there for alkali metal ion faujasites, the slope of the conductive part is typically about 2 orders of magnitude higher than that of the insulating regime, this representing a dramatic increase in conductivity. In this regard, the behavior of NaY(2.7) films is similar to that of a semiconductor junction. The breaking voltage and the rest of parameters may vary significantly from one zeolite to another. In fact, a detailed analysis of the electrical conductivity measurements for other zeolite films shows that there are remarkable differences that depend on the nature of the charge-balancing cation and the zeolitic structure. Figure 4 shows the differences in the $I-V$ plots for the series of alkali metal ion zeolites.

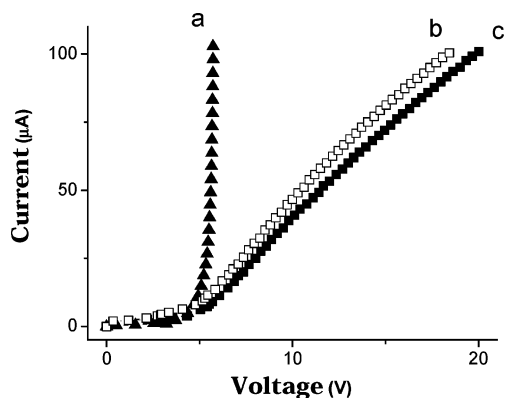


Figure 6. I - V plot to determine the influence of water in the electrical conductivity measurements: (a) NaY(2.7), (b) dehydrated CoY, and (c) hydrated CoY.

It is known³¹ that cobalt ions inside zeolites visually exhibit either a blue or pink color depending on their hydration state. Thus, we prepared two cells, one of them containing blue (dehydrated) and the second pink (hydrated) cobalt Y zeolite. The transparency of the ITO electrode permitted confirmation of the degree of hydration over the complete duration of the measurements. The actual I - V plots are presented in Figure 6, in which we have also included, for comparison, the profile of NaY(2.7). As can be seen there, the presence of water plays only a marginal influence, with hydration somewhat decreasing the electrical conductivity of the zeolite film.

Thus, the effect of the water content is not as large as that of other variables, such as the nature of the charge-balancing cation and the structure of the zeolite. Concerning Figure 6 and, specifically, the remarkable difference between the I/V curves of NaY(2.7) and CoY, the most probable explanation for the higher conductivity of NaY(2.7) is the higher charge density of Co^{2+} as compared to more mobile Na^+ and alkali metal ions. To disregard the presence of cobalt oxide species on the external zeolite surface that could disguise the conductivity measurements, an X-ray photoelectron spectroscopy analysis of Co revealed that this element is almost absent from the external surface of CoY. In addition, it is well-established that the blue/pink color is associated with the degree of hydration of the Co^{2+} ions. Other cobalt species, particularly oxides, are rather insensitive to the presence of moisture as compared to free ions. Thus, all the available data indicates that the different I/V profile between NaY(2.7) and CoY (either hydrated or dehydrated) is really reflecting the influence of the charge-balancing cation on the conductivity.

In fact, the zeolite structure is one of the most important parameters controlling the electrical conductivity of zeolite films. Figure 7 shows the profiles recorded for mordenite and ZSM-5 zeolites in their Na and H^+ forms. Also, for comparison purposes, the profile of NaY(2.7) was included in Figure 7.

Three general trends can be deduced from Figure 7, the first being that the films of zeolites in their H^+ form behave as resistors rather than semiconductors and are always less conductive than the Na^+ forms. This is in agreement with

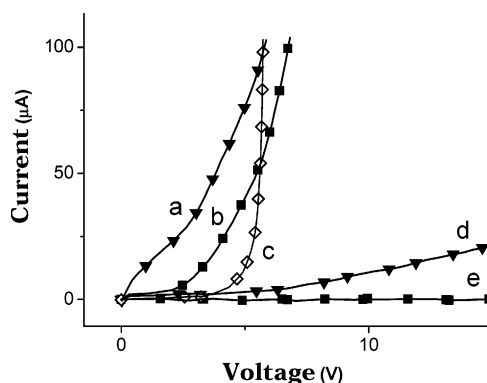


Figure 7. Electrical conductivity of the Na^+ and H^+ forms of ZSM-5 and mordenite zeolites: (a) Na ZSM-5, (b) Na mordenite, (c) NaY(2.7), (d) H^+ ZSM-5, and (e) H^+ mordenite.

the covalent nature of protons bonded to the ionic bond between the sodium ion and the framework. The second trend is that there is an optimum of the framework Si/Al ratio that makes the zeolite exhibit the maximum conductivity: a lower or higher Si/Al ratio plays a negative role in the conductivity of zeolite films. This optimum suggests the operation of two opposite factors, one increasing the conductivity as the Si/Al ratio increases and the other factor decreasing the conductivity as the Si/Al ratio increases. We speculate that the first of these two factors could be the population of sodium ions that increases when decreasing the Si/Al ratio, which should enhance the electrical conductivity, while the second factor could be the diffusion energy barrier that should be lower as the framework Si/Al ratio increases.

The third trend is that there are notable differences in the electrical conductivity pattern depending on the zeolite structure. While the reason for this different behavior is not clear at the present, we notice that, in addition to variations in the zeolite structure, other parameters such as the framework silicon/aluminum ratio, surface area, and particle size (see Table 1) are also varied from one zeolitic structure to another. The reason for this is that the synthesis of each zeolite structure requires a particular gel composition and synthesis conditions, giving particles of a preferred size for a certain surface area.^{32,33} In other words, when varying the zeolite structure, most of the other textural physicochemical parameters are also necessarily varied.

The data that have been presented clearly indicate that the nature of the zeolite film determines, to a large extent, its electrical conductivity. Thinking in terms of potential applications of these conductivity data in nanotechnology and considering the fact that in supramolecular host-guest systems most of the adsorbed material is incorporated inside the zeolite micropores, it is relevant to discuss whether the electrical conductivity measurements are a phenomenon occurring exclusively on the exterior of the zeolite particle or if they also involve some degree of intrazeolite charge transport.

In principle, the data available show that the electrical conductivity is somehow sensitive to the composition and properties of the intrazeolite space. The data supporting this

(31) Verberckmoes, A. A.; Weckhuysen, B. M.; Pelgrims, J.; Schoonheydt, R. A. *J. Phys. Chem.* **1995**, *99*, 15222-8.

(32) Russu, R. *Zeolites: Synthesis*; XXX: YYY, ZZZ, 1998; Vol. I.

(33) Thompson, R. W. *Mol. Sieves* **1998**, *1*, 1-33.

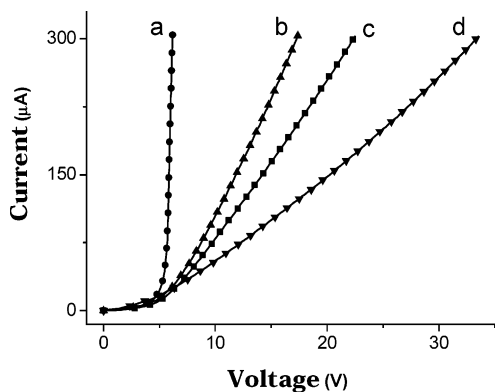


Figure 8. I - V plot of several $\text{Ru}(\text{bpy})_3^{2+}/\text{NaY}(2.7)$ samples at different external surface coverages: (a) 0%, (b) 10%, (c) 25%, and (d) 50%.

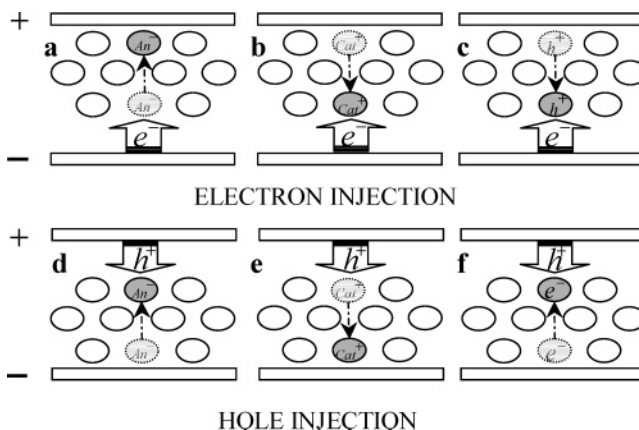
involvement of the zeolite intracrystalline space in the electrical conductivity are the following: (i) the sensitivity of the plot to the nature of the charge-balancing cations that are located in the intracrystalline space, (ii) the influence of the framework Si/Al ratio, (iii) the influence of the zeolite topology and pore size on the I - V plot, and (iv) the different behavior of amorphous nonporous silica and zeolites.

Evidence that the external surface is also influencing, to some extent, the electrical conductivity of the zeolite films was obtained by adsorbing a ruthenium trisbipyridyl complex on the external surface of the zeolite particles and observing some diminution in the electrical conductivity plots. It is well-known from the literature^{15,34,35} that ruthenium trisbipyridyl is size-excluded from the interior of the faujasite structure, and its adsorption can only occur on the exterior of the zeolite grains. Therefore, adsorption of ruthenium trisbipyridyl should alter the properties of the external surface without influencing the internal voids, and this should be reflected on the corresponding I - V plots of the $\text{Ru}(\text{bpy})_3^{2+}/\text{NaY}(2.7)$. The positive charges of $\text{Ru}(\text{bpy})_3^{2+}$ are also specially suited for adsorption in zeolites given the negative charge of their framework.

Aimed at determining the influence of the external surface, we prepared three $\text{Ru}(\text{bpy})_3^{2+}/\text{NaY}(2.7)$ samples at external surface coverages of approximately 10, 25, and 50%. It was considered that larger $\text{Ru}(\text{bpy})_3^{2+}$ -to- $\text{NaY}(2.7)$ ratios in the adsorption could lead to the formation of $\text{Ru}(\text{bpy})_3^{2+}$ crystals on the zeolite powder, rather than increasing the surface coverage by forming a monolayer on the zeolite particles. The electrical conductivity measurements of these three $\text{Ru}(\text{bpy})_3^{2+}/\text{NaY}(2.7)$ samples are presented in Figure 8 in which the response of pristine/ $\text{NaY}(2.7)$ has also been plotted for comparison.

From this figure, it can be concluded that the presence of $\text{Ru}(\text{bpy})_3^{2+}$ plays a negative influence on the electrical conductivity, converting the film from a semiconductor to a resistor depending on the $\text{Ru}(\text{bpy})_3^{2+}$ content. We believe that these significant variations in conductivity give an indication of the extent to which the external surface participates in the electrical conductivity measurements. However, we notice that the preferred location of $\text{Ru}(\text{bpy})_3^{2+}$ on the pore openings can also influence the intracrystalline

Scheme 1. Different Possibilities for Intrazeolite Electrical Conduction from External Working Electrodes to the Zeolite Interior^a



^a Top: one electron enters the zeolite accompanied by anion (a), cation (b), or hole (c) redistribution. Bottom: electrode hole injection accompanied by anion (d), cation (e), or electron (f) reorganization to maintain the electronegativity of the particle.

charge migration even when $\text{Ru}(\text{bpy})_3^{2+}$ is located externally. Although this large influence of the external surface in the electrical conductivity is not unexpected, it should also be stressed that the plots of Figures 4–6 corresponding to samples in which the external surface is essentially identical reflect the influence of the intrazeolite contribution to the electrical conductivity.

Concerning the actual intrazeolite charge transport mechanism, several possibilities can be envisioned at the moment, involving ion migration, electron or hole transport, or a combination of all of these as indicated in Scheme 1. Electrons and holes will be created when the potential difference between electrodes is sufficiently high to initiate a redox process and will be accompanied by cation redistribution.

According to the zeolite structure, charge injection from external electrodes into the zeolite film will be accompanied by a reaccommodation of mobile charge-balancing cations inside the zeolite micropores, so intrazeolitic ion mobility is an important factor that has to occur simultaneously in electron or hole injection. There are several precedents from the Mallouk, Dutta, and Kochi groups, among others, that have discussed in detail intracrystalline charge migrations.^{29,36–41} Also, the mechanisms of charge migration have been discussed by Bedouhi et al.,^{42,43} Rollison et al.,^{44–46} and

(36) Brigham, E. S.; Snowden, P. T.; Kim, Y. I.; Mallouk, T. E. *J. Phys. Chem.* **1993**, *97*, 8650–5.

(37) Kim, Y. I.; Mallouk, T. E. *J. Phys. Chem.* **1992**, *96*, 2879.

(38) Yonemoto, E. H.; Kim, Y. I.; Schmehl, R. H.; Wallin, J. O.; Shoulders, B. A.; Richardson, B. R.; Haw, J. F.; Mallouk, T. E. *J. Am. Chem. Soc.* **1994**, *116*, 10557.

(39) O'Neill, M. A.; Cozens, F. L.; Schepp, N. P. *J. Phys. Chem. B* **2001**, *105*, 12746–12758.

(40) Castagnola, N. B.; Dutta, P. K. *J. Photosci.* **1999**, *6*, 91–96.

(41) Yoon, K. B.; Park, Y. S.; Kochi, J. K. *J. Am. Chem. Soc.* **1996**, *118*, 12710–12718.

(42) Balkus, K. J.; Bedioui, F.; Roue, L.; Briot, E.; Devynck, J.; Bell, S. L. *J. Electroanal. Chem.* **1994**, *373*, 19–29.

(43) Devynck, J.; Bedioui, F. *J. Phys. IV* **1994**, *4*, 131–146.

(44) Rolison, D. R. *Chem. Rev.* **1990**, *90*, 867–878.

(45) Rolison, D. R. In *Stud. Surf. Sci. Catal.*; Jansen, J. C., Stöcker, M., Karge, M., Weitkamp, J., Eds.; Elsevier: Amsterdam, 1994; Vol. 85, p 543.

(34) Das, S. K.; Dutta, P. K. *Langmuir* **1998**, *14*, 5121–5126.

(35) Dutta, P. K.; Turbeville, W. J. *J. Phys. Chem.* **1992**, *96*, 9410–16.

us^{47,48} in the context of the electrochemistry of zeolite occluded guests. Our electrical conductivity measurements do not allow for distinguishing the different charge transport mechanisms indicated in Scheme 1. Further work is underway to clarify the actual charge transport by applying the Hall effect based on magnetic field effects on the charge transport.

In conclusion, by designing appropriate cells and performing electrical conductivity measurements under conditions that are relevant to the construction of nanotechnology devices, we have observed a typical semiconductor behavior for alkali metal ion Y faujasites, with an increase in the

conductivity of about 2 orders of magnitude at breaking voltages of about 4 V. $I-V$ plots are sensitive to the nature of the intracrystalline space and depend on the charge-balancing cation, framework Si/Al ratio, zeolite structure, and the characteristics of the external surface. All these data point toward a promising application of zeolite hosts as active layers in microelectronics in which voltages between 4 and 10 volts are typically applied and a certain conductivity of the material is required.

Acknowledgment. Financial support by the Spanish Ministry of Science and Technology (Grants MAT2003-01226 and MAT2004-06744) is gratefully acknowledged. J.F.C. and D.F. thank the Spanish Ministry of Science and Technology for a postgraduate research scholarship.

CM050467E

(46) Rolison, D. R.; Bessel, C. A. *Acc. Chem. Res.* **2000**, *33*, 737–744.

(47) Domenech, A.; Garcia, H.; Alvaro, M.; Carbonell, E. *J. Phys. Chem. B* **2003**, *107*, 3040–3050.

(48) Domenech, A.; Garcia, H.; Domenech-Carbo, M. T.; Galletero, M. S. *Anal. Chem.* **2002**, *74*, 562–569.